FRET Quenching of Photosensitizer Singlet Oxygen Generation

Jonathan F. Lovell,[†] Juan Chen,[‡] Mark T. Jarvi,[‡] Wei-Guo Cao,[§] Annette D. Allen,[||] Yuanqin Liu,[||] Thomas T. Tidwell,[||] Brian C. Wilson,[‡,⊥] and Gang Zheng*[,†,‡,⊥]

Institute of Biomaterials and Biomedical Engineering, Department of Medical Biophysics and Department of Chemistry, University of Toronto, Canada, Division of Biophysics and Bioimaging, Ontario Cancer Institute, Toronto, ON M5G 1L7, Canada, and Department of Chemistry, Shanghai University, China

Received: November 24, 2008; Revised Manuscript Received: December 29, 2008

The development of activatable photodynamic therapy (PDT) has demonstrated a utility for effective photosensitizer quenchers. However, little is known quantitatively about Forster resonance energy transfer (FRET) quenching of photosensitizers, even though these quenchers are versatile and readily available. To characterize FRET deactivation of singlet oxygen generation, we attached various quenchers to the photosensitizer pyropheophorbide-α (Pyro) using a lysine linker. The linker did not induce major changes in the properties of the photosensitizer. Absorbance and emission wavelength maxima of the quenched constructs remained constant, suggesting that quenching by ground-state complex formation was minimal. All quenchers sharing moderate spectral overlap with the fluorescence emission of Pyro ($J \geq 5.1 \times 10^{13}$ M^{-1} cm^{-1} nm^4) quenched over 90% of the singlet oxygen, and quenchers with weaker spectral overlap displayed minimal quenching. A self-quenched double Pyro construct exhibited intermediate quenching. Consistent with a FRET deactivation mechanism, extension of the linker to a 10 residue polyproline peptide resulted in only the quenchers with spectral overlap almost 2 orders of magnitude higher ($J \geq 3.7 \times 10^{15}$ M^{-1} cm^{-1} nm^4) maintaining high quenching efficiency. Overall, there was good correlation (0.98) between fluorescence quenching and singlet oxygen quenching, implying that fluorescence intensity can be a convenient indicator for the singlet oxygen production status of activatable photosensitizers. Uniform singlet oxygen luminescence lifetimes of the compounds, along with minimal triplet state transient absorption were consistent with quenchers primarily deactivating the photosensitizer excited singlet state. In vitro, cells treated with well-quenched constructs demonstrated greatly reduced PDT induced toxicity, indicating that FRET-based quenchers can provide a level of quenching useful for future biological applications. The presented findings show that FRET-based quenchers can potently decrease singlet oxygen production and therefore be used to facilitate the rational design of activatable photosensitizers.

Introduction

Photodynamic therapy (PDT) treats diseased regions of the body with the introduction of a photosensitizer followed by intense light irradiation onto a target area. The irradiation causes the photosensitizer to generate cytotoxic singlet oxygen that destroys cells through apoptosis or necrosis.[1] PDT has become a clinical treatment option for ophthalmic[2] and cancer-related diseases.[3] Although careful placement and delivery of the irradiation light confers a level of selectivity to PDT greater than most other disease treatments, PDT is still limited by damage it induces in adjacent healthy tissues. Furthermore, PDT is presently not an appropriate treatment for conditions in which diseased cells are not confined to a small and homogeneous region of the body.

To overcome limitations of PDT, approaches have been developed to further minimize damage the photosensitizer inflicts in nontarget cells. Photosensitizers that are cleared within hours, and not days, have been developed to prevent cutaneous phototoxicity after light treatment. However, rapidly clearing agents do not permit greater light dosage to be used nor prevent damage in tissue near the treatment site. Photoimmunotherapy relies on photosensitizer-conjugated antibodies to target cancer cells overexpressing certain cell surface markers.[4] This approach holds promise, but it is unclear how effectively the extracellular antigen−antibody complexes can be internalized so that the singlet oxygen generated by the photosensitizers may attack intracellular targets. An alternate approach of growing interest is the use of activatable photosensitizers.[5] These molecules usually contain a photosensitizer, a singlet oxygen quencher, and an active linker to regulate the activation of the photosensitizer. In the inactive state, the photosensitizer remains in a quenched conformation and generates only a small amount of singlet oxygen upon irradiation. Cleavage or extension of the linker by the target positions the photosensitizer further from the quencher and results in greater singlet oxygen generation. Bioactive linkers such as cleavable peptide substrates[6] or nucleic acids capable of hybridizing to specific mRNAs[7] have been shown to increase singlet oxygen production in response to biological targets. Other activatable photosensitizers have been developed that respond to pH[8] and to nanoparticle delivery.[9] Remarkably, in xenograft mouse models, protease-activated photosensitizers have been used in vivo to achieve recession or reduced growth of tumors.[10,11] The activatable photosensitizer concept has broad potential, since in theory many activatable

* To whom correspondence should be addressed. E-mail: Gang.Zheng@uhnres.utoronto.ca.
† Institute of Biomaterials and Biomedical Engineering, University of Toronto.
‡ Department of Medical Biophysics, University of Toronto.
§ Department of Chemistry, Shanghai University.
|| Department of Chemistry, University of Toronto.
⊥ Division of Biophysics and Bioimaging, Ontario Cancer Institute.

10.1021/jp810324v CCC: $40.75
Published on Web 02/12/2009

optical probes could be converted for PDT by substituting the fluorophore for a photosensitizer.[12] The benefits of activatable photosensitizers are negated if singlet oxygen reduction is not sufficient in the inactive conformation, resulting in killing of cells lacking the target. Correct quencher selection is therefore an important step in designing an activatable photosensitizer.

Previous examination of fluorophore quenchers on nucleic acid molecular beacons showed that effective fluorescence quenching occurred via both Forster resonance energy transfer (FRET) and through formation of ground-state complexes.[13] However, ground-state complex formation depends on sustained and direct contact between the photoactive molecule and the quencher, thus it is difficult to rationally design beacons relying on this mechanism. On the other hand, FRET may be predicted by spectral overlap and is effective within a predetermined range of fluorophore and quencher distances. Unlike conventional fluorophores, effective photosensitizers display a high singlet oxygen yield. Although there has been broad interest in quenching singlet oxygen generated by photosensitizers,[14] rather than FRET-based quenchers, most studies have focused on direct quenching of the generated singlet oxygen,[15] collisional quenching of the photosensitizer singlet[16] and triplet excited state,[17] and quenching by ground-state formation.[18] The efficiency that metal ions—well-known fluorophore quenchers[19]—can quench photosensitizers after covalent conjugation in a metal substituted porphyrin has been investigated.[20] Carbon nanotubes[21] and fullerenes[22] have also been explored as photosensitizer quenchers. It has been shown that photosensitizers themselves can act as FRET-based quenchers of quantum dots.[23,24] This suggests the fluorescence properties of photosensitizers can be leveraged like conventional fluorophores to use FRET-based quenchers to attenuate singlet oxygen production. To examine this hypothesis, we synthesized photosensitizers covalently attached to quenchers with varying degrees of spectral overlap and examined their photodynamic properties.

Experimental Section

Synthesis and Purification of Quenched Constructs. Synthesis of the quenched constructs was carried out as shown in Scheme 1. Lysine was conjugated to Rink resin (Novabiochem) after Fmoc deprotection of the resin with 20% piperidine in *N,N*-dimethylformamide (DMF) for 30 min. The amount of activated amine was quantified by the cleaved Fmoc absorbance at 300 nm ($\varepsilon = 7800\ M^{-1}\ cm^{-1}$). Resin was washed with DMF, and the lysine linker was conjugated to the resin using a 5-fold molar excess of Fmoc-lysine-(MTT)-OH (Novabiochem), 1-hydroxybenzotriazole (HOBT) (Sigma), and *O*-(benzotriazol-1-yl)-*N,N,N′,N′*-tetramethyluronium hexafluorophosphate (HBTU) (Sigma) for 3 h in DMF with 2% *N,N*-diisopropylethyl amine (DIPEA) at room temperature. After washing the resin with DMF, the MTT group on the lysine ε-amine was removed by incubation with 2% trifluoroacetic acid (TFA) in dichloromethane for 20 min. The resin was washed with DMF and Pyro (purified from biomass as described previously[25]) was conjugated to the lysine ε-amine using a 2 fold molar excess of HOBT and HBTU in 2% DIPEA overnight at room temperature. Free Pyro was washed from the solid phase with DMF, and the Fmoc-lysine(Pyro) resin was dried and stored at −20 °C.

To conjugate the various quenchers, the N-terminal Fmoc protecting group of the lysine was removed with 20% piperidine in DMF for 30 min. After washing the resin with DMF, 5-fold excess quencher was incubated with the resin overnight with 2% DIPEA at room temperature. Five fold excess HOBT and HBTU was included for quenchers conjugated via a carboxylic acid functional group. After conjugation, the resin was washed with DMF, and the constructs were cleaved from the resin using 95% TFA and 5% triisopropylsilane (TIS) for 1 h followed by filtration, removal of the solvent by evaporation, and resuspension of the compound in a small amount of DMSO. The following quenchers were used: Blackberry Quencher (BBQ)-

SCHEME 1: Solid phase synthesis scheme used to generate quenched photosensitizer. Lysine was first conjugated to Rink resin before labeling the N-terminus of lysine with the photosensitizer and the side chain amine with the quencher. Dabcyl is shown in this example

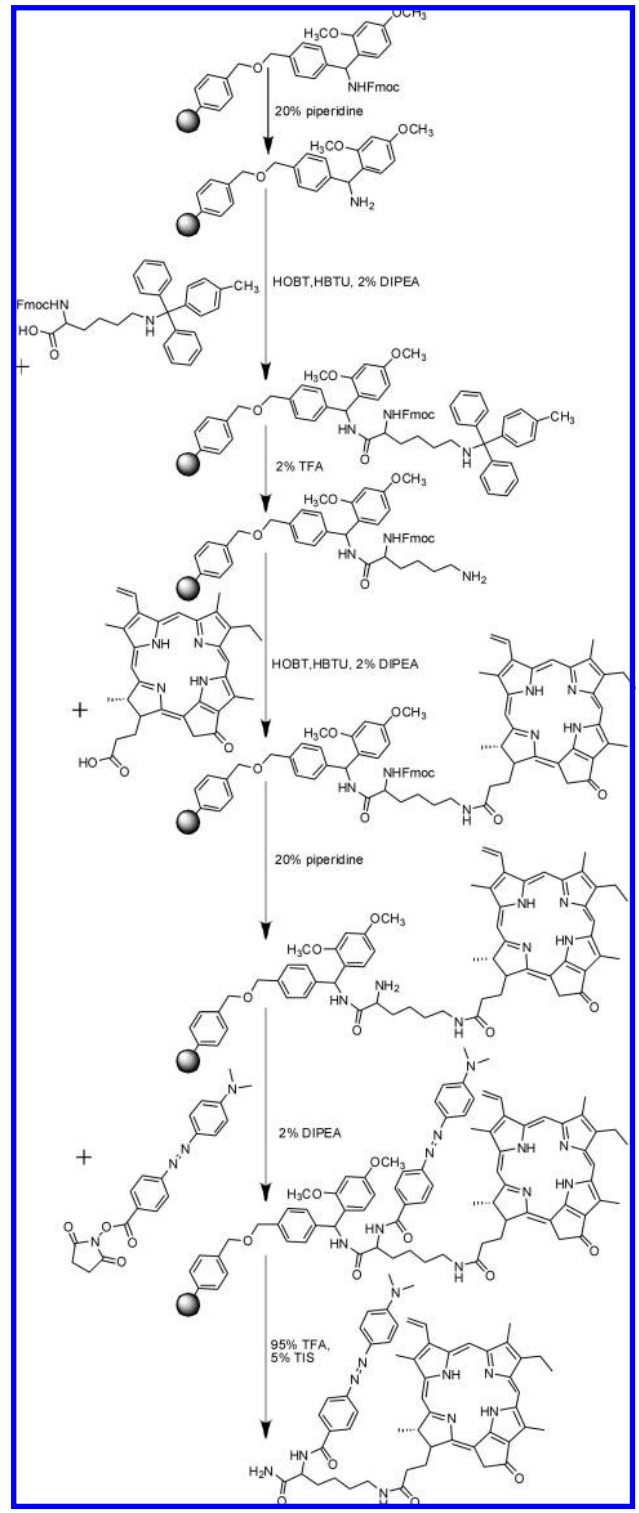

NHS (Berry Associates), Black Hole Quencher 1 (BHQ1)-NHS (Biosearch), Black Hole Quencher 3 (BHQ3)-NHS (Biosearch), Dabcyl (DAB)-COOH (Anaspec), Fmoc-tryptophan (TRP)-COOH (Novabiochem), and Disperse Blue 3-carboxylic acid (DB3)-COOH (synthesized as previously described[26]). Because of potential instability in 95% TFA, QXL-680-NHS (Anaspec) was conjugated in solution phase after cleavage of the Fmoc-lysine(Pyro) from the resin. All constructs were purified by HPLC using a Zorbax 300SB-C8 column (Agilent) with 0.1% TFA in water and acetonitrile as an eluant using a preparatory HPLC (Waters). The purified constructs were then identified using the same column and method on an analytical HPLC with a Micromass ESI mass spectrometry (Waters). To examine the effects of an extended spacer, a C-terminal lysine and 10 residue polyproline peptide (Fmoc-PPPPPPPPPPK(Mtt)) was synthesized with an automatic peptide synthesizer (Protein Science). After peptide synthesis, Fmoc deprotection with 20% piperidine in DMF and resin washing, Pyro was conjugated to the N-terminal of NH2-PPPPPPPPPPK(Mtt) on the solid-phase resin. The Pyro-labeled peptide was cleaved from the resin, and the lysine MTT protecting group was removed with 95% TFA and 5% TIS. Quenchers were then conjugated as described above. Constructs were then precipitated with diethyl ether and purified by HPLC, and the purity and identity were confirmed with HPLC-MS.

Photophysical Properties and Quantum Yields. Fluorescence decay profiles were recorded using a nanosecond time-correlated single-photon counting system (IBH). A solution of 500 nM compound in methanol was placed in a quartz cell and excited with a NanoLED ($\lambda_{ex} = 370$ nm), using an emission wavelength of 660 ± 16 nm at room temperature. Data was collected until 5000 counts accumulated in the maximum channel. Data was fit using the IBH software to a single exponential decay function. Triplet lifetimes were obtained by flashing a solution containing 5 μM argon-purged sample with a 308 nm laser. Spectra were collected 0.5 μs after the flash and represent the average of three measurements of the same samples. For triplet decay, the absorbance at 410 nm was monitored after flash and fit to a single exponential using the OriginPro 8 software (OriginLab).

Absorption spectra of the quenchers alone and the quenched constructs were measured in methanol on a spectrophotometer (Varian). To determine quantum yields, sample concentration was adjusted so the maximum absorbance was approximately 0.05, and the exact absorbance was recorded. Fluorescence quantum yields were calculated using eq 1.

$$\varphi_{F,SAMPLE} = \varphi_{F,REF} \times \frac{A_{REF}}{A_{SAMPLE}} \times \frac{F_{SAMPLE}}{F_{REF}} \quad (1)$$

$\phi_{F,SAMPLE}$ is the fluorescence quantum yield of the sample, and $\phi_{F,REF}$ is the reference fluorescence quantum yield of *meso*-tetraphenylporphyrin (TPP), taken as 0.13 in methanol.[27] A_{SAMPLE} is the absorbance at 410 nm of the quenched construct, and A_{REF} is the absorbance at 410 nm of the TPP. F_{SAMPLE} and F_{REF} correspond to the background-corrected emission spectra of the samples or TPP, integrated from 500 to 800 nm. Spectra were recorded on a Fluoromax fluorometer (Horiba Jobin Yvon) using 410 nm excitation and 3 nm excitation and emission slit widths. Because the quenchers displayed some absorbance at 410 nm, the fluorescence and singlet oxygen quantum yields of the quenched constructs were scaled by the following correction factors, based on the extinction coefficient at 410 nm of the quenchers compared to that of Pyro in methanol (97 000 $M^{-1}cm^{-1}$): BBQ: 1.07; BHQ1: 1.12; BHQ3: 1.12; DB3: 1.01; DAB: 1.19; QXL: 1.27. Where indicated, the Forster radius of the various quenchers was calculated using eq 2.

$$R_0 = 0.0211(\kappa^2 n^{-4} Q_D J(\lambda))^{1/6} \quad (2)$$

R_0 is the Forster radius, in nm. κ^2 represents the orientation factor, taken as 2/3. n is the refraction index of methanol, taken as 1.329; and Q_D is the fluorescence quantum yield of Pyro. The overlap integral, J, is described later in eq 6. Singlet oxygen quantum yields were calculated using eq 3.

$$\varphi_{\Delta,SAMPLE} = \varphi_{\Delta,REF} \times \frac{A_{REF}}{A_{SAMPLE}} \times \frac{^1O_2Counts_{SAMPLE}}{^1O_2Counts_{REF}} \quad (3)$$

$\phi_{\Delta,SAMPLE}$ is the singlet oxygen quantum yield of the sample, $\phi_{\Delta,REF}$ is the singlet oxygen quantum yield of Pyro, taken as 0.52.[28] A_{SAMPLE} is the absorbance at 410 nm of the construct, and A_{REF} is the Pyro absorbance at 410 nm. $^1O_2Counts_{SAMPLE}$ and $^1O_2Counts_{REF}$ are the background-corrected singlet oxygen counts of the sample and reference, respectively. Quantum yields were calculated with the average of 3−4 sample preparations.

The singlet oxygen counts and lifetimes were assessed by direct measurement of singlet oxygen luminescence as described previously.[29] In brief, the samples were irradiated with 523 nm light from a 10 ns pulsed frequency-doubled, Q-switched Nd:YLF laser operating at a repetition rate of 10 kHz, and the luminescence signal was detected with a near-infrared sensitive photomultiplier tube (H9170−45, Hamamatsu). The luminescence emission spectra were sampled using five bandpass filters (10 nm width) centered at 1210, 1240, 1270, 1300, and 1330 nm. At each filter, the signal was acquired for 200 000 laser pulses, and two cycles of the five filters were performed. The time-resolved luminescence signal was integrated from 0.5 to 40 microseconds for each filter at a time resolution of 100 ns. The singlet oxygen luminescence signal was calculated by subtracting the average of the integrated counts from the 1210, 1240, 1300, and 1330 nm filters from the integrated signal collected with the 1270 nm filter.

To determine the singlet oxygen luminescence lifetimes of the various samples, the time-resolved data was fit with the following well-known three-parameter equation using nonlinear least-squares fitting with OriginLab software.

$$L_{1270}(t) = A\frac{\tau_D}{\tau_T - \tau_D}\left[\exp\left(-\frac{t}{\tau_T}\right) - \exp\left(-\frac{t}{\tau_D}\right)\right] \quad (4)$$

$L(t)$ is the observed luminescence signal as a function of time. A is a constant that incorporates the extinction coefficient and quantum yield of the photosensitizer as well as the irradiance, τ_D is the singlet oxygen decay lifetime, and τ_T is the photosensitizer triplet state lifetime.

Photosensitizer Bleaching. The samples were dissolved in a mixture of 50% methanol in water, at a concentration of 2.5 μM. Fluorescence and singlet oxygen were monitored while the samples were irradiated continuously with the 523 nm laser. Singlet oxygen luminescence was collected as described above. The fluorescence was collected with a SMA fiber optic collimator into a 400 μm diameter fiber optic that delivered the light to a spectrometer (USB2000, Ocean Optics, USA) with a

580 nm long-pass filter in front of the collimator. The fluorescence was integrated from 650 to 670 nm. The irradiance was 110 mW cm^{-2}, and the total final radiant exposure was 116 J cm^{-2}. Experiments were performed with three separate samples.

Cell Viability Assay. Human nasopharynx carcinoma KB-1 cells were seeded and grown for 2 days in a 96 well plate (2.5×10^4 cells per well) before incubation with RPMI-1640 media containing 10% FBS and 1 μM construct in 0.5% DMSO and 0.2% TWEEN-80 (Sigma). After 16 h incubation at 37 °C in a 5% CO_2 incubator, the media was replaced with normal media, and the cells were then treated with PDT with 3 different light fluences (1, 5, or 10 Jcm^{-2}) using a 667 nm laser with a 130 $mWcm^{-2}$ fluence rate with 8, 40, and 80 s treatment times. Twenty-four hours later, cell viability was assessed by incubating 100 μL of 0.5 mg/mL MTT tracer, 3-(4,5-dimethylthiazol-2-yl)-2,5-diphenyltetrazolium bromide (Invitrogen), with the cells for 1 h. After removing the MTT, cells were resuspended in 200 uL of DMSO, and the absorbance of the MTT was measured at 560 nm. Cell viability was calculated using eq 5.

$$\text{Viability} = \frac{A_S - A_B}{A_N - A_B} \times 100\% \quad (5)$$

A_B is the absorbance at 560 nm of the MTT in a blank well, A_N is the absorbance of cells at 560 nm without any drug or light treatment, and A_S is the absorbance at 560 nm of the well of interest. Averages and standard deviations were based on seven experiments.

Results and Discussion

Generation of Quenched Constructs. To examine the quenching of pyropheophorbide-α (Pyro), a conjugation scheme was developed to hold the photosensitizer and quencher together with a lysine residue. A solid phase synthesis was used to simplify the purification process. The linker alone, TRP, DAB, Pyro, BHQ1, BBQ, BHQ3, and QXL-680 were conjugated to Pyro, generating Pyro−Link, Pyro−TRP, Pyro−DAB, Pyro−Pyro, Pyro−BHQ1, Pyro−BBQ, Pyro−BHQ3, and Pyro−QXL, respectively. Synthesis was carried out as described in the experimental section, and Scheme 1 shows the typical synthesis procedure for Pyro−DAB as an example. The final products were purified by preparatory HPLC, the purity of the compounds was confirmed by analytical HPLC, and their correct identities were confirmed by mass spectrometry (Figure 1 of the Supporting Information).

The basic photophysical properties of Pyro−Link were investigated and compared to Pyro alone. Figure 1A shows that Pyro and Pyro−Link had nearly indistinguishable fluorescence excitation and emission spectra, with the excitation spectra characterized by the Soret band at 410 nm and Q-band at 663 nm, and the emission spectra displaying a 672 nm maxima with a minor shoulder at 725 nm. As shown in Figure 1B and Table 1, Pyro with and without the linker displayed a monoexponential fluorescence lifetime of 6.2 and 6.3 ns, respectively. The observed single exponential fluorescence lifetimes of Pyro and Pyro−Link were close to a previously reported modified Pyro lifetime of 6.5 ns.[30] Triplet state lifetimes were measured using laser photolysis (Figure 1C) monitoring the recovery of the Soret band. The observed triplet lifetimes of Pyro and Pyro−Linker were 54.2 and 51.5 μs, respectively. These triplet lifetimes were longer but comparable to a reported triplet lifetime of 35 μs for a modified Pyro.[31] The similar photophysical properties of Pyro and Pyro−Link show the linker did not induce major changes in the characteristics of the photosensitizer.

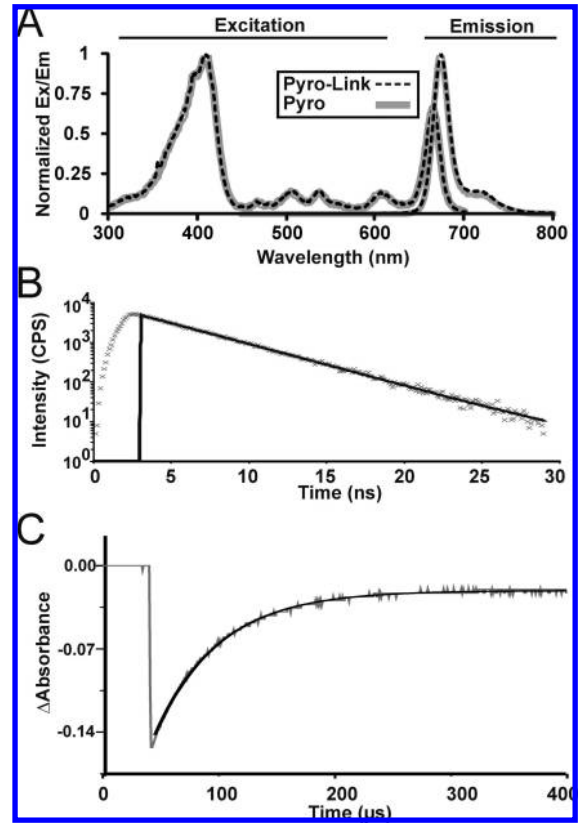

Figure 1. Properties of Pyro−Link. (A) Normalized excitation and emission spectra of 500 nM Pyro−Link (black, dashed lines) and Pyro (gray line) in methanol. (B) Fluorescence lifetime of Pyro−Link. Grey marks indicate observed data and the black line shows the single exponential fit. (C) Triplet lifetime of Pyro−Link under argon. The gray line indicates observed absorbance at 410 nm (corresponding to recovery of the Soret band) and the black curve shows the single exponential fit.

TABLE 1: Properties of Pyro−linker and Pyro

	singlet lifetime	X^2	triplet lifetime	R^2
Pyro−Link	6.4 ns	0.995	54.2 us	0.998
Pyro	6.3 ns	0.978	51.5 us	0.995

To determine if FRET can be used to effectively deactivate a photosensitizer, the quenching efficiency of several quenchers with varying degrees of spectral overlap with Pyro fluorescence emission was investigated. The quenchers used were Dabcyl-NHS (DAB), Black Hole Quencher 1-NHS (BHQ1), Disperse Blue 3-COOH (DB3), Blackberry quencher-NHS (BBQ), Black Hole Quencher 3-NHS (BHQ3) and QXL-680-NHS (QXL). They absorbed in different ranges between 450 and 750 nm, as shown in Figure 2A by the normalized absorption spectra of the quenchers. The quenchers shared varying degrees of overlap with Pyro fluorescence emission, which is represented by the shaded gray box covering 90% of the total Pyro fluorescence output. Figure 2B shows the absorption spectra of two constructs, Pyro−Link and Pyro−BBQ. FRET efficiency is related to the spectral overlap integral J, which depends on not only the wavelength range of overlap, but also the extinction coefficient of the acceptor, and may be calculated using eq 6.

$$J(\lambda) = \frac{\int_0^\infty F_D(\lambda)\varepsilon_A(\lambda)\lambda^4 \, d\lambda}{\int_0^\infty F_D(\lambda) \, d\lambda} \quad (6)$$

$F_D(\lambda)$ is the emission spectra of Pyro, $\varepsilon_A(\lambda)$ is the extinction coefficient of the acceptor in M^{-1} cm^{-1}, and λ is the wavelength in nm. As shown in Table 2, the quenchers covered a broad range of J values. QXL, with an absorption peak well aligned with Pyro fluorescence emission and a large extinction coefficient of 128 000 M^{-1} cm^{-1}, has an overlap integral on the order of 10^{16} M^{-1} cm^{-1} nm^4. Conversely, TRP displayed only trace absorbance in the Pyro emission range and has an overlap integral almost 5 orders of magnitude less than QXL. The structures of the quenchers conjugated to Pyro are shown in Figure 3 (except for the QXL structure, which was not given by the manufacturer). The linker separated the Pyro and quencher by 5 carbon atoms and 2 amide bonds. This spacer was chosen to emulate the close spacing of an activatable photosensitizer where the quencher and photosensitizer are held together by self-folding, as seen in nucleic acid beacons (a concept that can be extended to peptide-based beacons[32]), or by hydrophobic interactions between the photosensitizer and quencher. All constructs were fairly hydrophobic and were soluble in methanol. DAB, BBQ, BHQ1, and BHQ3 contained N═N azo groups, BHQ1 and BBQ both contained nitro groups, and DB3 contained a quinine group. The absorbance spectra of the constructs are shown in Figure 2 of the Supporting Information.

Photosensitizer Quenching. Deactivation of the photosensitizer excited singlet state should reduce the number of excited photosensitizer molecules available to enter the triplet state and consequently lower singlet oxygen generation. The deactivation of the singlet excited-state of Pyro was evaluated by examining the fluorescence emission of the constructs. Figure 4A shows the fluorescence emission spectra in methanol of three constructs at 500 nM concentration: Pyro−Link, Pyro−Pyro, and Pyro−DB3. Although the self-quenched Pyro−Pyro displayed an 80% reduction in fluorescence, the Pyro−DB3 quenched 95% of the Pyro emission. Quenching of singlet oxygen generation was assessed directly by near-infrared luminescence of singlet oxygen. Figure 4B shows the 1270 nm peak of the singlet oxygen generated by the same constructs. A similar quenching trend was seen with Pyro−Pyro producing 60% less singlet oxygen than Pyro−Link and the Pyro−DB3 producing 93% less. The quenching summary for the entire set of constructs is shown in Table 3. Even though some quenched constructs displayed highly reduced emission intensity, the shape of the emission

TABLE 2: Properties of Quenchers

quencher	J (M^{-1} cm^{-1} nm^4)	abs max (nm)	ε (M^{-1} cm^{-1})
tryptophan (TRP)	3.8×10^{11}	280	9000
dabcyl (DAB)	1.2×10^{13}	454	32 000
BHQ1	5.1×10^{13}	521	38 000
DB3	5.0×10^{14}	639	19 000
BBQ	3.7×10^{15}	601	40 700
BHQ3	6.5×10^{15}	654	42 700
QXL	2.2×10^{16}	680	128 000

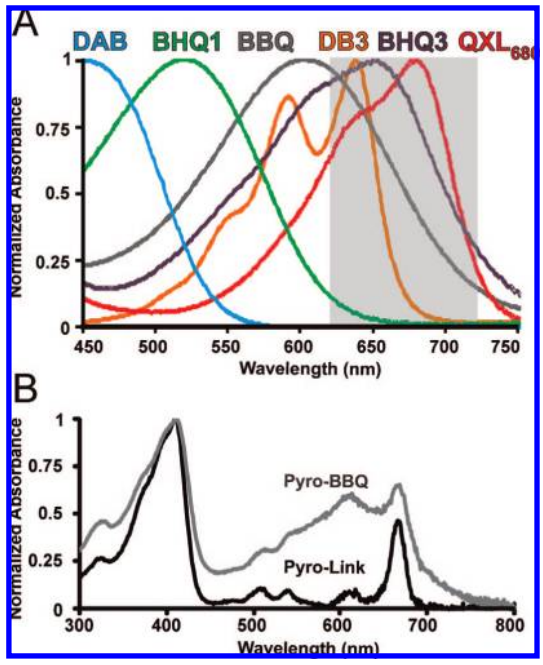

Figure 2. Normalized absorption spectra of quenchers and constructs. (A) Normalized absorption spectra of quenchers in methanol. The quenchers are labeled in the same order that the respective absorption maxima wavelength appears. The trace of DAB is shown in cyan, BHQ1 in green, BBQ in gray, DB3 in orange, BHQ3 in purple, and QXL in red. The transparent gray rectangle corresponds to the wavelength range representing 90% of Pyropehophorbide emission, centered around the fluorescence emission maximum. (B) Normalized absorption spectra of the two indicated constructs in methanol. Absorption spectra for all constructs are shown in Figure 2 of the Supporting Information.

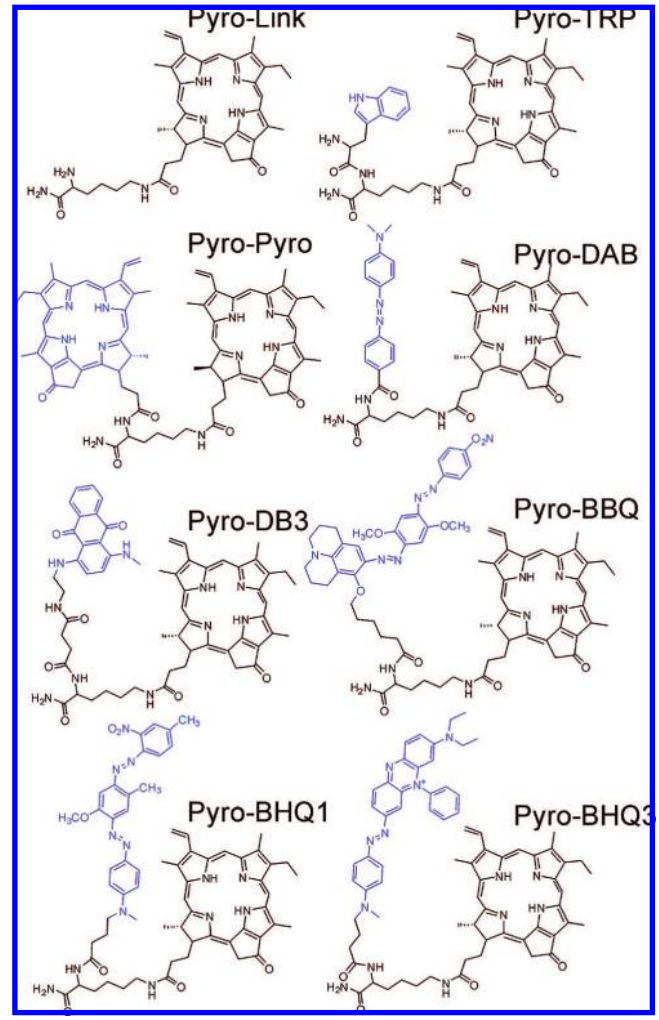

Figure 3. Structures of the various quenched constructs. The quenching moiety is shown in blue.

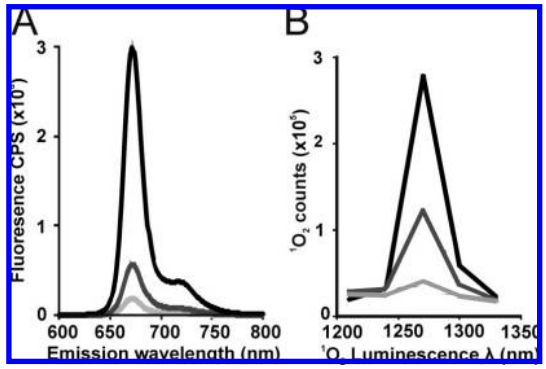

Figure 4. Pyro−Pyro displays intermediate quenching between Pyro−Link and Pyro−DB3. (A) Fluorescence emission spectra and (B) singlet oxygen luminescence of Pyro−Link (black), Pyro−Pyro (medium gray), and Pyro−DB3 (light gray).

spectra was constant, with an emission peak maximum of 672 nm. The absorption maximum also remained constant near 411 nm for almost all the quenched constructs. The constant absorption, as well as the constant emission maxima of the constructs, suggests that quenching by ground-state complex formation was minimal, since ground-state complexes display highly altered absorption properties.[13] Pyro−Pyro was the only construct to show a significantly altered absorption profile. The blue-shifted 398 nm Pyro−Pyro absorption maxima is consistent with self-stacking or aggregation of Pyro, which is a phenomenon observed previously with porphyrins that displayed the same wavelength shift upon aggregation.[33] Activatable probes that rely on self-quenching have been used extensively for in vivo imaging[34] and have advantages that they tend to have an easier synthesis protocol, and they also generate more signal per probe. However, these data indicate there may be a tradeoff in the quenching efficiency in the inactive state compared to FRET quencher based activatable photosensitizers.

Dabcyl, a common quencher that has relatively little ($J = 1.2 \times 10^{13}$ M^{-1} cm^{-1} nm^4) spectral overlap with Pyro fluorescence emission, quenched 33% of the Pyro fluorescence emission and 46% of the singlet oxygen generation. While reducing half the singlet oxygen production may be useful for some cases, a higher level of singlet oxygen attenuation that minimizes background photosensitization is desirable for in vivo applications. Quenchers with spectral overlap greater or equal to $J = 5.1 \times 10^{13}$ M^{-1} cm^{-1} nm^4 were the most efficient, reducing upward of 90% of the photosensitizer fluorescence and singlet oxygen production. Plotting the observed quantum yields as a function of Forster radius (Figure 5) shows the quenchers that had more overlap (and larger Forster radius) than Dabcyl were able to quench Pyro fluorescence and singlet oxygen yields with high efficiency. It was observed that after reaching a 90% threshold of fluorescence and singlet oxygen quenching (achieved with BHQ1) there was no further a clear relationship between spectral overlap and quenching, potentially due to variability in dipole alignment.

There was strong correlation between fluorescence and singlet oxygen quenching for the constructs. The Pearson's correlation coefficient between ϕ_F and ϕ_Δ for the values shown in Table 3 was 0.98, suggesting the two quantum yields were linked. Correlation between the fluorescence and singlet oxygen quantum yields is consistent with FRET-induced singlet state deactivation being the principle determinant of singlet oxygen generation inhibition for these constructs. However, differences between the extent of fluorescence and singlet oxygen quenching show that fluorescence and singlet oxygen are subject to different quenching processes, and the latter may be affected by factors including triplet state quenching or singlet oxygen scavenging. Those may have been factors for BHQ1 and BBQ, two quenchers that displayed greater than expected singlet oxygen attenuation. Those two quenchers were the only ones to contain a nitro group, a well-known quencher[35] that may have some conferred additional singlet oxygen quenching capacity.

Because the rigidity of the linker was unknown, it was difficult to ascribe how much of the singlet state deactivation process was due to FRET and how much was due to collisional quenching. Although these measurements were performed in the nanomolar range, and collisional quenching is usually observed at the millimolar scale during quencher titrations, the linker may increase the rate of contact between the Pyro and the quencher. Direct assessment of meaningful Stern−Volmer constants by quencher titrations was not possible due to the heavy optical interference of micromolar amounts of quencher with fluorescence and singlet oxygen measurements. To assess the extent of collisional quenching, we examined the construct quenched by tryptophan, a well-known collisional quencher.[36−38] This construct displayed negligible fluorescence and singlet oxygen quenching (2% and −5%, respectively), showing that collisional quenching was not a major deactivation pathway for Pyro−TRP and therefore was likely not a major factor for the deactivation of other constructs either.

To confirm FRET was the primary deactivation mechanism, we synthesized and purified constructs with the single lysine linker extended by a 10 residue polyproline peptide (Figure 6A). Polyproline was selected as the linker since it has frequently been used in FRET experiments as a spectroscopic ruler.[39] Fluorescence and singlet oxygen yields were measured and are shown in Figure 6B, as a function of Forster radius. While BHQ1 and DB3 could efficiently quench Pyro singlet oxygen when separated by a single lysine linker, these quenchers did not maintain effective Pyro quenching upon extension of the linker and increased separation from the photosensitizer. However, the three remaining quenchers with larger Forster radii—BBQ, BHQ3, and QXL—maintained greater than 90% quenching of fluorescence and singlet oxygen. The simulated values of fluorescence quantum yield are shown for two different linker lengths using eq 7.

$$\varphi_{F,simulated} = \frac{r^6 \cdot \varphi_{F,unquenced}}{r^6 + R_0^6 \cdot \varphi_{F,unquenched}} \quad (7)$$

$\phi_{F,simulated}$ is the simulated quantum yield, $\phi_{F,unquenched}$ is the quantum yield of Pyro, R_0 is the variable Forster radius, and r is the hypothetical distance between the quencher and fluorophore. The simulated traces show the quenched fluorescence quantum yield for $r = 1.9$ and 3.1 nm. 1.9 nm corresponds to the expected length of the 10 residue proline linker in methanol,[40] and 3.1 nm is the expected polyproline length in water,[41] shown for reference. The actual separation was likely slightly greater than 1.9 nm, since the distance to the centers of the quencher and photosensitizer dipoles, along with the extra lysine residue used for conjugation, contributed to the total separation, in addition to the polyproline spacing. The observed quantum yields followed a similar pattern as the simulated quenched fluorescence quantum yields. However, as with the single lysine linker, the effective Forster radius of the quenchers appeared less than predicted since the observed quenching was lower than expected. Despite having ample spectral overlap, the quenchers with the greatest Forster radius could not completely quench

TABLE 3: Properties of Quencher Constructs[a]

compound	abs max (nm)	em max (nm)	ϕ_F	% F quenching	ϕ_Δ	% Δ quenching
Pyro	411	672	0.49 (0.018)	2	0.52 (ref)	−5
Pyro−Link	411	672	0.50 (0.032)	0	0.49 (0.034)	0
Pyro−TRP	412	672	0.49 (0.049)	1	0.53 (0.063)	−5
Pyro−DAB	411	672	0.33 (0.049)	33	0.27 (0.051)	46
Pyro−Pyro	398	672	0.098 (0.029)	80	0.20 (0.0029)	60
Pyro−BHQ1	414	673	0.023 (0.002)	95	0.006 (0.002)	99
Pyro−DB3	411	674	0.025 (0.003)	95	0.034 (0.00032)	93
Pyro−BBQ	411	672	0.007 (0.0042)	99	0.013 (0.0048)	97
Pyro−BHQ3	410	673	0.023 (0.004)	95	0.036 (0.036)	93
Pyro−QXL	413	671	0.018 (0.015)	96	0.047 (0.019)	91

[a] Standard deviations in brackets.

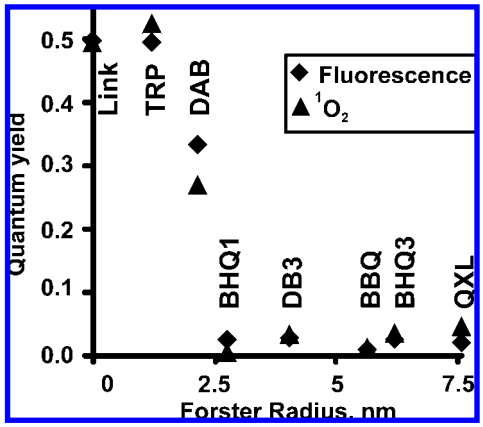

Figure 5. Quantum yields of constructs plotted as a function of quencher Forster radius. Fluorescence quantum yields are shown as diamonds, and singlet oxygen quantum yields are marked as triangles (measured in methanol).

Pyro, with the maximum achieved quenching between 90 and 95%, while the predicted values were close to 100% for a quenchers with simulated Forster radius values greater than 5 nm and $r = 1.9$ nm. Nonideal dipole alignment may have contributed to the lack of complete energy transfer.

The fluorescence and singlet oxygen quantum yields of the extended linker constructs had strong correlation (Pearson's correlation coefficient between ϕ_F and $\phi_\Delta = 0.99$), in line with an excited singlet state deactivation mechanism. Because activatable photosensitizers ultimately are intended for PDT, knowing how the singlet oxygen production responds to activation is essential. However, direct measurement of singlet oxygen is not always possible and often requires uncommon equipment and protocols. The data presented here suggest that measurement of the fluorescence of activatable photosensitizers is a good indicator for singlet oxygen status since the fluorescence response and singlet oxygen response was similar with quenchers of varying degrees of efficiency. Although not a substitute for direct singlet oxygen measurement, estimating singlet oxygen production status through fluorescence may allow activatable photosensitizers to be conveniently characterized with standard equipment such as fluorometers and fluorescence microscopes.

In some potential beacon designs, activation does not lead to complete separation of the photosensitizer and quencher. For instance, when a nucleic acid molecular beacon unfolds, the quencher and fluorophore still remain connected on the same molecule. In some circumstances, a quencher and photosensitizer predicted to have a very large Forster radius should be avoided, since it is possible that the activated and unfolded beacon still may be separated by a distance less than the quencher Forster

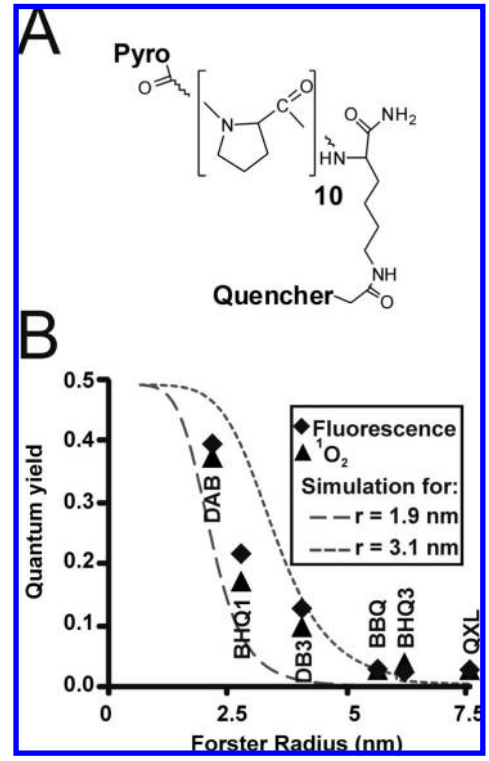

Figure 6. Structure and quantum yields of extended linker constructs. (A) Structure of the 10 residue polyproline linker. (B) Quantum yields of constructs plotted as a function of quencher Forster radius of the 10 residue polyproline linked constructs. Fluorescence quantum yields are shown as diamonds, and singlet oxygen quantum yields are marked as triangles (measured in methanol). Simulated values of fluorescence quenching are shown as dashed lines for two different distances as a function of Forster radius.

radius. This could lead to quenching of the photosensitizer even in the activated state and would reduce the activated signal increase. Selection of photosensitizer quenchers must therefore be planned carefully. A guideline based on the results observed here would be to assume a quencher Forster radius of 5 nm is required for linker separations of ~2 nm and a quencher Forster radius of 2.5 nm is required for shorter linker separations of less than ~1 nm.

Quenching Occurs Upstream of Singlet Oxygen Generation. Excluding ground-state complex formation, singlet oxygen quenching can be achieved by at least three pathways: deactivating the photosensitizer singlet state; deactivating the photosensitizer triplet state; and/or by directly scavenging singlet oxygen. It has previously been shown that a caretenoid quencher can quench singlet oxygen generation by all the above three ways when covalently attached to Pyro.[42] We examined whether or not FRET-based quenchers act as singlet oxygen scavengers.

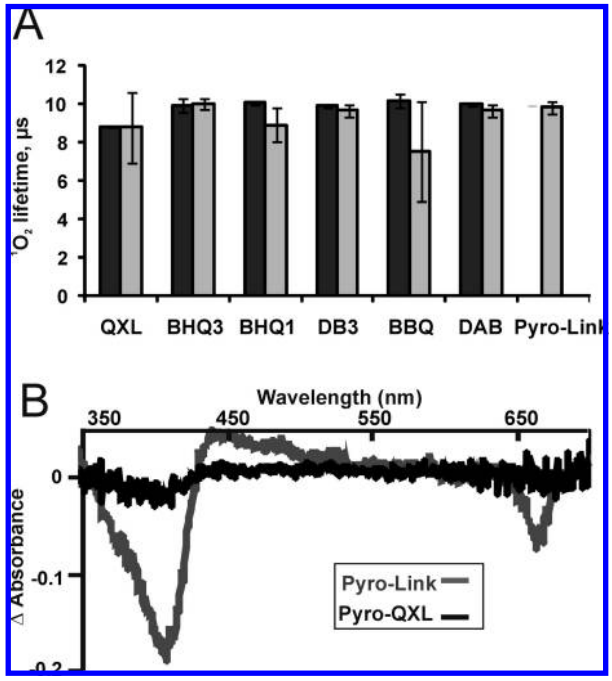

Figure 7. (A) Singlet oxygen luminescence lifetimes of the various compounds measured in methanol. Dark gray bars represent polyproline-linked compounds and light gray bars indicate single lysine-separated compounds. (B) Triplet state difference spectra of 5 μM Pyro−Link and Pyro−QXL, recorded under argron-purged methanol after flashing sample with 308 nm laser.

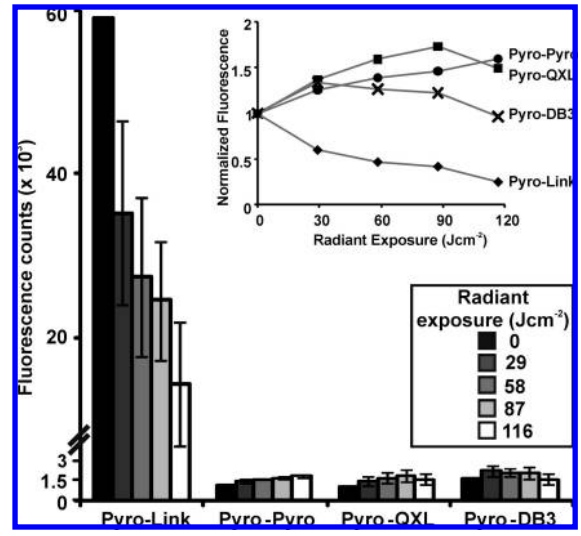

Figure 8. Bleaching of quenched constructs. 2.5 μM samples were continually irradiated with the amount of radiant exposure indicated in the legend and fluorescence emission was monitored over time. Upper right inset shows the normalized fluorescence emission as a function of cumulative exposure for Pyro−Link (diamonds), Pyro−DB3 (crosses), Pyro−QXL (squares), and Pyro−Pyro (circles).

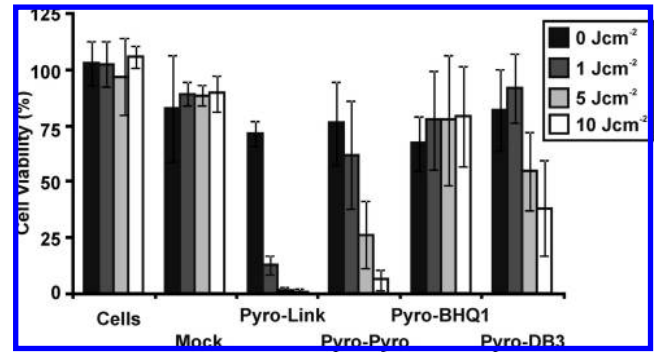

Figure 9. MTT viability assay. Cells were treated with 1 μM of various compounds followed by PDT using the laser exposure indicated in the legend. Mock treated cells were incubated with 0.5% DMSO and 0.2% TWEEN-80 alone. Viability was assessed 24 h after irradiation with the MTT assay.

The singlet oxygen lifetimes of various constructs were measured in methanol. As shown in Figure 7A, all the constructs displayed a singlet oxygen luminescence lifetime of approximately 10 μs. The singlet oxygen lifetimes of some well-quenched samples, such as Pyro−BBQ, were difficult to fit due to the very low singlet oxygen signal, resulting in large error bars in the measurement. Consistent with a singlet excited-state deactivation model, and in contrast to the previously reported caretenoid quencher, the uniformity of the quenched construct lifetimes indicates that FRET-based quenchers were not effective singlet oxygen scavengers. The triplet state difference spectra for Pyro−Link and a quenched construct, Pyro−QXL are shown in Figure 7B. It is apparent that the triplet state of Pyro lacks the Soret band absorption at 410 nm, resulting in the negative absorbance in the difference spectra. Pyro−Link had a triplet state difference absorption at the measurement time of 0.5 μs after the flash, showing that a portion of the constructs remained in the excited triplet state. However the QXL-quenched construct did not display any meaningful difference spectra, indicating the quenched construct had already returned to the singlet state by the time the spectra was recorded after the flash, consistent with FRET-induced singlet state deactivation of the triplet state.

Photobleaching. Photosensitizers may be subjected to extended light exposure. Continued irradiation of activatable photosensitizers could result in the photosensitzer or quencher losing efficiency over time due to photobleaching. Figure 8 illustrates that, without quencher, Pyro underwent photobleaching upon extended irradiation, resulting in a greater than 70% loss of fluorescence emission. On the other hand, the quenched constructs appeared to be resistant to photobleaching, and extended irradiation actually resulted in an increase in photosensitizer fluorescence. The increased fluorescence production was likely due to singlet-oxygen-induced damage to the quencher or direct photobleaching of the quencher. Although this phenomenon would reduce specificity of the activatable photosensitizer during PDT, compared to Pyro, the fluorescence and corresponding singlet oxygen production was still an order of magnitude less for the quenched constructs investigated. For QXL, the total singlet oxygen production after 116 J cm^{-2} remained less than 5% of that for Pyro, showing the quenched constructs would still deliver a high level of selectivity.

Suitability for Cells. An advantage of activatable photosensitizers is that they can be delivered to both target and nontarget cells, and only the target cells will activate and dequench the photosensitizer. However, if the quenching is ineffective, a large number of nontarget cells will also be killed, negating the benefits of the activatable PDT. To examine if the singlet oxygen production of the quenched constructs was sufficiently attenuated to prevent toxicity with PDT treatment, 1 μM compound was incubated with human nasopharyngeal carcinoma-derived KB cells, PDT was performed, and cell viability was assessed. Figure 9 shows cell viability after treatment with various compounds with an increasing laser irradiation dose. Mock treated cells showed a small loss in viability, although there was no response to increasing light dose, suggesting the DMSO and TWEEN delivery formulation had a mild inhibitory effect on cell viability. When incubated with the unquenched Pyro−Link construct, viability was reduced to 12% of the untreated control

cells with the 1 J cm^{-2} light dose treatment. The 5 and 10 J cm^{-2} treatments killed almost all the cells, resulting in only 1.3% and 0.6% cell viability, respectively. Pyro−Pyro, which exhibited 60% singlet oxygen quenching efficiency was 80% less effective than Pyro−Link at killing cells at the 1 J cm^{-2} radiant exposure. The DB3 quenched construct, which had 93% quenched singlet oxygen yield, displayed even less toxicity than the self-quenched construct. Cells treated with Pyro−BHQ1, which displayed 99% singlet oxygen quenching, displayed no PDT light dose response. At the highest light dosage of 10 J cm^{-2}, Pyro−Pyro, Pyro−DB3, and Pyro−BHQ1 displayed 9-, 57-, and 118-fold reduced toxicity, respectively, when compared with Pyro−Link. The inhibited toxicity of the quenched photosensitizers shows that the degree of quenching achieved is sufficient for maintaining a harmless inactive quenched state.

Conclusion

We have demonstrated that FRET-based quenchers can be used to quench photosensitizer singlet oxygen generation. For effective quenching, the amount of required spectral overlap varies based on the conformation of the photosensitizer and quencher. For activatable photosensitizers where the quencher is located within a few nanometers to the photosensitizer, only moderate spectral overlap is required, and using a quencher with increased spectral overlap may not further decrease fluorescence and singlet oxygen generation beyond 90%. However, if the photosensitizer and quencher are positioned further away, as may be the case for peptide-based activatable photosensitizers, the amount of spectral overlap required from the quencher increases as the linker length increases to maintain efficient singlet oxygen quenching. On the basis of the results observed, to ensure the FRET-based photosensitizer quencher is highly effective, a quencher Forster radius of 5 nm is required for linker separations of ∼2 nm and a quencher Forster radius of 2.5 nm is required for shorter subnanometer linker separations. The quenching of fluorescence and singlet oxygen was similar, not only suggesting the primary deactivation pathway was from the photosensitizer singlet state, but also showing that fluorescence can be used as an indicator of singlet oxygen production status for activatable probes. Activatable photosensitizers hold potential for basic biochemical research and future therapeutics and the findings presented here show that FRET-based quenchers can be used to facilitate their design.

Acknowledgment. This work was supported by grants from the Canadian Cancer Society through the National Cancer Institute of Canada (No. 018510 to G.Z. and No. 014245 to B.C.W.), the Canadian Institute of Health Research (No. 179821 to G.Z.), and the Joey and Toby Tanenbaum/Brazilian Ball Chair in Prostate Cancer Research (G.Z.). Thanks to Professor Mitch Winnik for assistance with fluorescence lifetime measurements. Thanks also to Tracy Liu and Pui-Chi Lo for assistance with PDT.

Supporting Information Available: Purity and mass of constructs as well as their normalized absorption spectra are included. This material is available free of charge via the Internet at http://pubs.acs.org.

References and Notes

(1) Dougherty, T. J.; Gomer, C. J.; Henderson, B. W.; Jori, G.; Kessel, D.; Korbelik, M.; Moan, J.; Peng, Q. *J. Natl. Cancer. Inst.* **1998**, *90*, 889–905.

(2) Woodburn, K. W.; Engelman, C. J.; Blumenkranz, M. S. *Retina* **2002**, *22*, 391–405.

(3) Brown, S. B.; Brown, E. A.; Walker, I. *Lancet Oncol.* **2004**, *5*, 497–508.

(4) van Dongen, G. A. M. S.; Visser, G. W. M.; Vrouenraets, M. B. *Adv. Drug. Deliv. Rev.* **2004**, *56*, 31–52.

(5) Clo, E.; Snyder, J. W.; Ogilby, P. R.; Gothelf, K. V. *ChemBioChem* **2007**, *8*, 475–481.

(6) Chen, J.; Stefflova, K.; Niedre, M. J.; Wilson, B. C.; Chance, B.; Glickson, J. D.; Zheng, G. *J. Am. Chem. Soc.* **2004**, *126*, 11450–11451.

(7) Chen, J.; Lovell, J. F.; Lo, P.; Stefflova, K.; Niedre, M.; Wilson, B. C.; Zheng, G. *Photochem. Photobiol. Sci.* **2008**, *7*, 775–781.

(8) McDonnell, S. O.; Hall, M. J.; Allen, L. T.; Byrne, A.; Gallagher, W. M.; O'Shea, D. F. *J. Am. Chem. Soc.* **2005**, *127*, 16360–16361.

(9) McCarthy, J. R.; Perez, J. M.; Brückner, C.; Weissleder, R. *Nano. Lett.* **2005**, *5*, 2552–2556.

(10) Zheng, G.; Chen, J.; Stefflova, K.; Jarvi, M.; Li, H.; Wilson, B. C. *Proc. Natl. Acad. Sci.* **2007**, *104*, 8989–8994.

(11) Choi, Y.; Weissleder, R.; Tung, C. *Cancer. Res.* **2006**, *66*, 7225–7229.

(12) Lovell, J. F.; Zheng, G. *J. Innov. Opt. Health. Sci.* **2008**, *1*, 45–61.

(13) Marras, S. A. E.; Kramer, F. R.; Tyagi, S. *Nucleic Acids Res.* **2002**, *30*, e122.

(14) Schweitzer, C.; Schmidt, R. *Chem. Rev.* **2003**, *103*, 1685–1757.

(15) Kanofsky, J. R. *Photochem. Photobiol.* **1990**, *51*, 299–303.

(16) Z Zhang, L. Z.; Tang, G. *J. Photochem. Photobiol. B* **2004**, *74*, 119–125.

(17) Lambert, C. R.; Kochevar, I. E. *Photochem. Photobiol.* **1997**, *66*, 15–25.

(18) Dunn, D. A.; Lin, V. H.; Kochevar, I. E. *Photochem. Photobiol.* **1991**, *53*, 47–56.

(19) Rupcich, N.; Chiuman, W.; Nutiu, R.; Mei, S.; Flora, K. K.; Li, Y.; Brennan, J. D. *J. Am. Chem. Soc.* **2006**, *128*, 780–790.

(20) McCarthy, J. R.; Weissleder, R. *ChemMedChem* **2007**, *2*, 360–365.

(21) Zhu, Z.; Tang, Z.; Phillips, J.; Yang, R.; Wang, H.; Tan, W. *J. Am. Chem. Soc.* **2008** *130*, 10856−10857.

(22) Guldi, D. M.; Maggini, M.; Menna, E.; Scorrano, G.; Ceroni, P.; Marcaccio, M.; Paolucci, F.; Roffia, S. *Chemistry* **2001**, *7*, 1597–1605.

(23) Samia, A. C. S.; Chen, X.; Burda, C. *J. Am. Chem. Soc.* **2003**, *125*, 15736–15737.

(24) Tsay, J. M.; Trzoss, M.; Shi, L.; Kong, X.; Selke, M.; Jung, M. E.; Weiss, S. *J. Am. Chem. Soc.* **2007**, *129*, 6865–6871.

(25) Zheng, G.; Li, H.; Zhang, M.; Lund-Katz, S.; Chance, B.; Glickson, J. D. *Bioconjug. Chem.* **2002**, *13*, 392–396.

(26) May, J. P.; Brown, L. J.; van Delft, I.; Thelwell, N.; Harley, K.; Brown, T. *Org. Biomol. Chem.* **2005**, *3*, 2534–2542.

(27) Bonnett, R.; McGarvey, D. J.; Harriman, A.; Land, E. J.; Truscott, T. G.; Winfield, U. J. *Photochem. Photobiol.* **1988**, *48*, 271–276.

(28) Hackbarth, S.; Ermilov, E.; Roder, B. *Opt. Commun.* **2004**, *248*, 295–305.

(29) Niedre, M. J.; Secord, A. J.; Patterson, M. S.; Wilson, B. C. *Cancer. Res.* **2003**, *63*, 7986–7994.

(30) Kelbauskas, L.; Dietel, W. *Photochem. Photobiol.* **2002**, *76*, 686–694.

(31) Delanaye, L.; Bahri, M. A.; Tfibel, F.; Fontaine-Aupart, M.; Mouithys-Mickalad, A.; Heine, B.; Piette, J.; Hoebeke, M. *Photochem. Photobiol. Sci.* **2006**, *5*, 317–325.

(32) Jiang, T.; Olson, E. S.; Nguyen, Q. T.; Roy, M.; Jennings, P. A.; Tsien, R. Y. *Proc. Natl. Acad. Sci.* **2004**, *101*, 17867–17872.

(33) Kano, K.; Fukuda, K.; Wakami, H.; Nishiyabu, R.; Pasternack, R. F. *J. Am. Chem. Soc.* **2000**, *122*, 7494–7502.

(34) Weissleder, R.; Tung, C. H.; Mahmood, U.; Bogdanov, A. *Nat. Biotechnol.* **1999**, *17*, 375–378.

(35) Green, S. A.; Simpson, D. J.; Zhou, S. G.; Ho, P. S.; Blough, N. V. *J. Am. Chem. Soc.* **1990**, *112*, 7337–7346.

(36) Daraio, M. E.; Volker, A.; Aramendia, P. F.; Roman, E. S. *Photochem. Photobiol.* **1997**, *67*, 371–377.

(37) Michaeli, A.; Feitelson, J. *Photochem. Photobiol.* **1994**, *59*, 284–289.

(38) Marmé, N.; Knemeyer, J.; Sauer, M.; Wolfrum, J. *Bioconjug. Chem.* **2003**, *14*, 1133–1139.

(39) Stryer, L.; Haugland, R. P. *Proc. Natl. Acad. Sci.* **1967**, *58*, 719–726.

(40) Kakinoki, S.; Hirano, Y.; Oka, M. *Polymer Bulletin* **2005**, *53*, 109–115.

(41) Schuler, B.; Lipman, E. A.; Steinbach, P. J.; Kumke, M.; Eaton, W. A. *Proc. Natl. Acad. Sci.* **2005**, *102*, 2754–2759.

(42) Chen, J.; Jarvi, M.; Lo, P.; Stefflova, K.; Wilson, B. C.; Zheng, G. *Photochem. Photobiol. Sci.* **2007**, *6*, 1311–1317.

JP810324V